

Prospects of monoclinic Yb:KLu(WO₄)₂ crystal for multi-watt microchip lasers

Josep Maria Serres,¹ Pavel Loiko,^{1,2} Xavier Mateos,^{1,*}
Konstantin Yumashev,² Nikolai Kuleshov,² Valentin Petrov,³
Uwe Griebner,³ Magdalena Aguiló,¹ and Francesc Díaz¹

¹Física i Cristal·lografia de Materials i Nanomaterials (FiCMA-FiCNA), Universitat Rovira i Virgili (URV),
Campus Sescelades, c/ Marcel·li Domingo, s/n., Tarragona, E-43007, Spain

²Center for Optical Materials and Technologies, Belarusian National Technical University,
65/17 Nezavisimosti Ave., Minsk, 220013, Belarus

³Max Born Institute for Nonlinear Optics and Short Pulse Spectroscopy, 2A Max-Born-Str.,
Berlin, D-12489, Germany
xavier.mateos@urv.cat

Abstract: The concept of Yb-doped double tungstate microchip lasers is verified and scaled to the multi-watt power level. The active element is a 2.6 mm-thick Yb:KLuW crystal cut along the N_g optical indicatrix axis. Maximum continuous-wave output power of 4.4 W is extracted at 1049 nm with a slope efficiency of 65% and an optical-to-optical efficiency of 44% with respect to the absorbed pump power. The laser emission is linearly polarized and the intensity profile is characterized by a near-circular TEM₀₀ mode with $M^2_{x,y} < 1.1$. Due to low intracavity losses of the microchip laser, laser operation at wavelengths as long as 1063 nm is achieved. The mechanism of the thermal mode stabilization in the microchip cavity is confirmed. At very low resonator losses polarization-switching between $E \parallel N_m$ and N_p oscillating states is observed and explained on the basis of spectroscopic and thermal lens characteristics.

©2015 Optical Society of America

OCIS codes: (140.3380) Laser materials; (140.6810) Thermal effects; (140.3480) Lasers, diode-pumped.

References and links

1. J. J. Zayhowski and A. Mooradian, "Single-frequency microchip Nd lasers," *Opt. Lett.* **14**(1), 24–26 (1989).
2. J. J. Zayhowski and C. Dill III, "Diode-pumped passively Q-switched picosecond microchip lasers," *Opt. Lett.* **19**(18), 1427–1429 (1994).
3. T. Taira, A. Mukai, Y. Nozawa, and T. Kobayashi, "Single-mode oscillation of laser-diode-pumped Nd:YVO₄ microchip lasers," *Opt. Lett.* **16**(24), 1955–1957 (1991).
4. V. Petrov, M. C. Pujol, X. Mateos, O. Silvestre, S. Rivier, M. Aguiló, R. M. Solé, J. Liu, U. Griebner, and F. Díaz, "Growth and properties of KLu(WO₄)₂, and novel ytterbium and thulium lasers based on this monoclinic crystalline host," *Laser & Photon. Rev.* **1**(2), 179–212 (2007).
5. M. Pollnau, Y. E. Romanyuk, F. Gardillou, C. N. Borca, U. Griebner, S. Rivier, and V. Petrov, "Double tungstate lasers: from bulk toward on-chip integrated waveguide devices," *IEEE J. Sel. Top. Quantum Electron.* **13**(3), 661–671 (2007).
6. X. Mateos, R. Sole, J. Gavaldà, M. Aguiló, J. Massons, F. Díaz, V. Petrov, and U. Griebner, "Crystal growth, spectroscopic studies and laser operation of Yb³⁺-doped potassium lutetium tungstate," *Opt. Mater.* **28**(5), 519–523 (2006).
7. M. C. Pujol, M. A. Bursukova, F. Guell, X. Mateos, R. Sole, J. Gavaldà, M. Aguiló, J. Massons, F. Díaz, P. Klopp, U. Griebner, and V. Petrov, "Growth, optical characterization, and laser operation of a stoichiometric crystal KYb(WO₄)₂," *Phys. Rev. B* **65**(16), 165121 (2002).
8. O. Silvestre, J. Grau, M. C. Pujol, J. Massons, M. Aguiló, F. Díaz, M. T. Borowiec, A. Szewczyk, M. U. Gutowska, M. Massot, A. Salazar, and V. Petrov, "Thermal properties of monoclinic KLu(WO₄)₂ as a promising solid state laser host," *Opt. Express* **16**(7), 5022–5034 (2008).
9. S. Biswal, S. P. O'Connor, and S. R. Bowman, "Thermo-optical parameters measured in ytterbium-doped potassium gadolinium tungstate," *Appl. Opt.* **44**(15), 3093–3097 (2005).
10. J. Liu, V. Petrov, X. Mateos, H. Zhang, and J. Wang, "Efficient high-power laser operation of Yb:KLu(WO₄)₂ crystals cut along the principal optical axes," *Opt. Lett.* **32**(14), 2016–2018 (2007).

11. P. A. Loiko, V. E. Kisel, N. V. Kondratuk, K. V. Yumashev, N. V. Kuleshov, and A. A. Pavlyuk, "14 W high-efficiency diode-pumped cw Yb:KGd(WO₄)₂ laser with low thermo-optic aberrations," *Opt. Mater.* **35**(3), 582–585 (2013).
12. J. E. Hellstrom, S. Bjurshagen, and V. Pasiskevicius, "Laser performance and thermal lensing in high-power diode-pumped Yb:KGW with athermal orientation," *Appl. Phys. B* **83**(1), 55–59 (2006).
13. J. Liu, V. Petrov, H. Zhang, and J. Wang, "Power scaling of a continuous-wave and passively Q-switched Yb:KLu(WO₄)₂ laser end-pumped by a high-power diode," *Appl. Phys. B* **88**(4), 527–530 (2007).
14. U. Griebner, S. Rivier, V. Petrov, M. Zorn, G. Erbert, M. Weyers, X. Mateos, M. Aguiló, J. Massons, and F. Diaz, "Passively mode-locked Yb:KLu(WO₄)₂ oscillators," *Opt. Express* **13**(9), 3465–3470 (2005).
15. S. Pekarek, C. Fiebig, M. C. Stumpf, A. E. H. Oehler, K. Paschke, G. Erbert, T. Südmeyer, and U. Keller, "Diode-pumped gigahertz femtosecond Yb:KGW laser with a peak power of 3.9 kW," *Opt. Express* **18**(16), 16320–16326 (2010).
16. G. Palmer, M. Schulze, M. Siegel, M. Emons, U. Bunting, and U. Morgner, "Passively mode-locked Yb:KLu(WO₄)₂ thin-disk oscillator operated in the positive and negative dispersion regime," *Opt. Lett.* **33**(14), 1608–1610 (2008).
17. P. A. Loiko, K. V. Yumashev, N. V. Kuleshov, V. G. Savitski, S. Calvez, D. Burns, and A. A. Pavlyuk, "Thermal lens study in diode pumped N_g- and N_p-cut Nd:KLu(WO₄)₂ laser crystals," *Opt. Express* **17**(26), 23536–23543 (2009).
18. A. S. Grabtchikov, A. N. Kuzmin, V. A. Lisinetskii, V. A. Orlovich, A. A. Demidovich, M. B. Danailov, H. J. Eichler, A. Bednarkiewicz, W. Strek, and A. N. Titov, "Laser operation and Raman self-frequency conversion in Yb:KYW microchip laser," *Appl. Phys. B* **75**(6-7), 795–797 (2002).
19. V. G. Savitski, R. B. Birch, E. Fraczek, A. J. Kemp, P. A. Loiko, K. V. Yumashev, N. V. Kuleshov, and A. A. Pavlyuk, "The prospects for Yb- and Nd-doped tungstate microchip lasers," in *CLEO/Europe-EQEC 2013, Munich, May, 12–16, 2013*, P. CA-10.5.
20. P. A. Loiko, J. M. Serres, X. Mateos, K. V. Yumashev, N. V. Kuleshov, V. Petrov, U. Griebner, M. Aguiló, and F. Diaz, "Thermal lensing in Yb:KLu(WO₄)₂ crystals cut along the optical indicatrix axes," *Laser Phys. Lett.* **11**(12), 125802 (2014).
21. J. M. Serres, X. Mateos, P. Loiko, K. Yumashev, N. Kuleshov, V. Petrov, U. Griebner, M. Aguiló, and F. Diaz, "Diode-pumped microchip Tm:KLu(WO₄)₂ laser with more than 3 W of output power," *Opt. Lett.* **39**(14), 4247–4250 (2014).
22. S. Chenais, F. Druon, S. Forget, F. Balembois, and P. Georges, "On thermal effects in solid-state lasers: The case of ytterbium-doped materials," *Prog. Quantum Electron.* **30**(4), 89–153 (2006).
23. H. Zhao and A. Major, "Orthogonally polarized dual-wavelength operation of a CW Yb:KGW laser Induced by thermal lensing," in *CLEO Technical Digest* (OSA, 2013), P. CTh4I.2.
24. F. Druon, M. Olivier, A. Jaffrès, P. Loiseau, N. Aubry, J. DidierJean, F. Balembois, B. Viana, and P. Georges, "Magic mode switching in Yb:CaGdAlO₄ laser under high pump power," *Opt. Lett.* **38**(20), 4138–4141 (2013).
25. P. Loiko, F. Druon, P. Georges, B. Viana, and K. Yumashev, "Thermo-optic characterization of Yb:CaGdAlO₄ laser crystal," *Opt. Mater. Express* **4**(11), 2241–2249 (2014).
26. P. A. Loiko, X. Mateos, N. V. Kuleshov, A. A. Pavlyuk, K. V. Yumashev, V. Petrov, U. Griebner, M. Aguiló, and F. Diaz, "Thermal-lens-driven effects in N_g-cut Yb- and Tm-doped monoclinic KLu(WO₄)₂ crystals," *IEEE J. Quantum Electron.* **50**, 669–676 (2014).
27. T. Taira, J. Saikawa, T. Kobayashi, and R. L. Byer, "Diode-pumped tunable Yb:YAG miniature lasers at room temperature: modeling and experiment," *IEEE Select. Topics Quantum Electron.* **3**(1), 100–104 (1997).
28. J. Dong, A. Shirakawa, K. Ueda, H. Yagi, T. Yanagitani, and A. A. Kaminskii, "Efficient Yb³⁺:Y₃Al₅O₁₂ ceramic microchip lasers," *Appl. Phys. Lett.* **89**(9), 091114 (2006).
29. M. Tsunekane and T. Taira, "300 W continuous-wave operation of a diode edge-pumped, hybrid composite Yb:YAG microchip laser," *Opt. Lett.* **31**(13), 2003–2005 (2006).
30. P. Dekker, J. M. Dawes, J. A. Piper, Y. Liu, and J. Wang, "1.1 W CW self-frequency-doubled diode-pumped Yb:YAl₃(BO₃)₄ laser," *Opt. Commun.* **195**(5-6), 431–436 (2001).
31. J. Dong, K. Ueda, and A. A. Kaminskii, "Efficient passively Q-switched Yb:LuAG microchip laser," *Opt. Lett.* **32**(22), 3266–3268 (2007).
32. P. Peterson, A. Gavrielides, T. C. Newell, N. Vretenar, and W. P. Latham, "ASE in thin disk lasers: theory and experiment," *Opt. Express* **19**(25), 25672–25684 (2011).

1. Introduction

The microchip laser concept opens up new opportunities for diode-pumped solid-state lasers. It implies a laser crystal with two flat mirrors attached or directly coated on its endfaces, resulting in a compact setup insensitive to misalignment and a low loss cavity [1]. The extension of this idea can be the insertion of a saturable-absorber for passive Q-switching with the benefit of short pulse generation [2]. Microchip lasers can be also designed for single-longitudinal-mode operation by insertion of a Fabry-Perot etalon in the cavity [3]. The ytterbium (Yb) ion is well-known for its emission around 1 μm, characterized by simple energy level scheme eliminating parasitic processes, reduced non-radiative path, extremely low quantum defect and the possibility of diode pumping with commercial diodes operating

around ~980 nm. Thus, the combination of these two features in Yb-doped microchip lasers is favorable for highly efficient laser operation at medium power levels.

Among the Yb-doped materials, monoclinic double tungstates, DTs, with the chemical formula $KRE(WO_4)_2$ with $RE = Gd, Y$ or Lu , attract enormous attention [4,5]. Yb:DTs possess intense and wide absorption and emission bands with strong polarization anisotropy (due to low-symmetry structure) [6]. They permit high doping levels, up to 100 at.%, without significant distortion of the lattice and luminescence quenching (the latter is mainly related to the large $RE^{3+}-RE^{3+}$ separation) [7]. Although the thermal conductivity of these crystals is moderate (~3 W/mK) [8], their thermo-optical properties can be improved within the athermal cut concept [9]. In recent years, all three representatives of the DT family, shortly KGdW, KYW and KLuW, were studied for incorporation of Yb and highly efficient lasing in continuous-wave (CW) [10–12], Q-switched [13] and mode-locked [14–16] regimes. The stoichiometric KYbW crystal was successfully investigated as well [7]. The KLuW host seems to be best suited for laser applications due to the nearly perfect matching of ionic radii of optically “passive” Lu^{3+} (0.977 Å) and laser-active Yb^{3+} (0.985 Å).

Although the laser performance of Yb:DTs was intensively studied, they were rarely employed in microchip lasers. The reason is the negative thermal lens for crystals cut along the growth direction [17], the *b*-axis (so-called “standard” cut; typically used for commercial lasers). The first microchip laser, containing a “standard”-cut 10 at.%Yb:KYW crystal, yielded only 55 mW of CW output at 1025 nm with a slope efficiency of 23%. In this work Q-switched operation was also demonstrated [18]. The negative thermal lens was identified as the limitation for further laser optimization. Later, the Yb:KYW microchip performance was improved with output power reaching up to 0.8 W in the CW mode and a slope efficiency of 41% [19] by using a thin (250 μm) active element, “sandwiched” in a synthetic diamond for better heat removal. Although the crystal was cut along the N_g -axis of the optical indicatrix, resulting in a positive lens, this complex design did not allow one to further increase the output power and reach the high slope efficiencies inherent for Yb:DT lasers. Thus, achieving of high-power and highly efficient microchip laser operation of Yb:DTs is still a challenging task. In the present paper, we demonstrate an efficient multi-watt Yb:KLuW microchip laser based on “bulk” crystal geometry.

2. Experimental

For the present study, we used a 3 at.%Yb:KLuW crystal grown by the Top-Seeded-Solution Growth (TSSG) slow-cooling method. The actual ion density measured by Electron Probe Micro Analysis (EPMA) was 1.8×10^{20} at/cm³ (2.9 at.%). From the as-grown bulk, we cut a rectangular sample oriented for propagation along the N_g -axis of the optical indicatrix (2.60 mm-thick) with the cross-section of $3.05(N_m) \times 2.73(N_p)$ mm². Both crystal faces spanned by the N_m and N_p axes ($m \times p$) were polished to laser quality; they were uncoated. The crystal was mounted in a Cu-holder providing cooling from all four lateral sides and Indium foil ensured the thermal contact. The holder was water-cooled down to 14 °C.

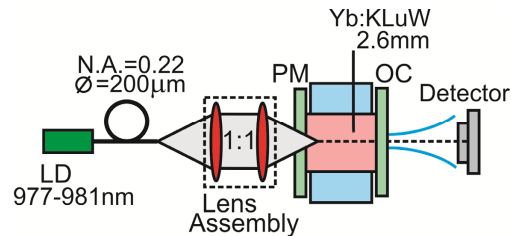


Fig. 1. Scheme of the compact Yb:KLuW microchip laser; LD: laser diode, PM: pump mirror, OC: output coupler.

The plano-plano cavity of the microchip laser, Fig. 1, consisted of a pump mirror (PM) antireflection (AR)-coated for the spectral range 880–990 nm and high-reflection (HR)-coated for 1015–1230 nm, and an output coupler (OC) providing transmittances $T_{OC} = 1, 5$ or 10%

for 1020–1100 nm. Both mirrors were attached directly to the polished crystal faces without air gaps keeping the cavity length at 2.60 mm, the geometrical length of the Yb:KLuW sample. As pump source, we used an InGaAs fiber coupled laser diode (fiber core diameter: 200 μm ; numerical aperture N.A.: 0.22) delivering up to 20 W output power in the spectral range between 977 and 981 nm, depending on the current level. The unpolarized pump radiation was collimated and focused into the crystal using a lens assembly (1:1 imaging ratio, 30 mm focal length) resulting in a pump spot radius w_p in the crystal of $\sim 100 \mu\text{m}$. No pump bleaching of the crystal absorption was observed. As all the three OCs provide partial reflection at the pump wavelength ($\sim 95\%$, 90% and 80% , respectively), the crystal was pumped in a double-pass. The measured single-pass absorption in the crystal was 43–53%, depending on the diode current level.

3. Results and discussion

Figure 2 presents the power transfer characteristics of the CW Yb:KLuW microchip laser. A maximum output power of 4.4 W is obtained for $T_{\text{OC}} = 10\%$ connected to the maximum slope efficiency of 65%, calculated with respect to the overall absorbed diode power. The input-output dependence is linear, indicating no detrimental influence of thermal loading in the crystal on the laser performance. The laser threshold is 2.1 W of absorbed pump power and the optical-to-optical efficiency amounts to 44%. The performance of the microchip laser for $T_{\text{OC}} = 5\%$ is very similar to 10%, with a slightly reduced slope efficiency of 62%. The laser polarization in both cases was linear, $\mathbf{E} \parallel N_m$. No change of the polarization state was observed for the entire pump range. The inset in Fig. 2 shows two intensity profiles of the output beam captured in the far-field just above the laser threshold ($P_{\text{abs}} = 3 \text{ W}$) and at the highest pump level ($P_{\text{abs}} = 10 \text{ W}$), recorded with a FLIR SC7210 thermal imaging camera. The far-field intensity profiles are near-circular and exhibit Gaussian shape for both directions, $\parallel N_p$ and $\parallel N_m$. The measured $M^2_{x,y}$ factors ($x \equiv p$, $y \equiv m$) are < 1.1 , indicating no degradation of the quality of the laser beam.

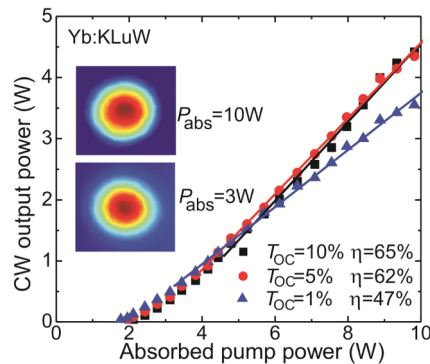


Fig. 2. Input-output characteristics of the CW Yb:KLuW microchip laser for different T_{OC} (symbols: experimental data, lines: calculated slope, η), inset: spatial intensity profiles of the output beam.

In order to explain the mechanism of mode stabilization in the Yb:KLuW microchip cavity, we characterize the thermal lens in the N_g -cut crystal, see Fig. 3(a). Here symbols represent direct measurements for $\mathbf{E} \parallel N_m$, for details see [20]. Lines denote the calculation of the so-called sensitivity factor of the thermal lens M , amounting to $+ 3.5$ and $+ 2.8 \text{ m}^{-1}/\text{W}$ for directions $\parallel N_p$ and $\parallel N_m$, respectively. Thus, the thermal lens in a N_g -cut crystal is strong and purely positive, which enables the stabilization of the laser mode in a plano-plano cavity. In Fig. 3(b) the calculated radius of the laser mode w_1 is plotted vs. the absorbed pump power for a “hot” cavity. The line for $w_p = 100 \mu\text{m}$ is added to analyze the mode-matching conditions. The increase of pump power leads to stronger positive lens and the value of w_1 is reduced. For $P_{\text{abs}} > 4 \text{ W}$ the reduction of w_1 is only marginal and near 9 W, it is stabilized around 55 ± 5

μm . This mode mismatch is the main reason for the somewhat reduced slope efficiency observed for our Yb:KLuW microchip laser as compared to the highest value of $>80\%$ achieved for CW diode-pumped Yb:DTs [10]. Recently, a similar behavior was observed also for a Tm:KLuW microchip laser [21].

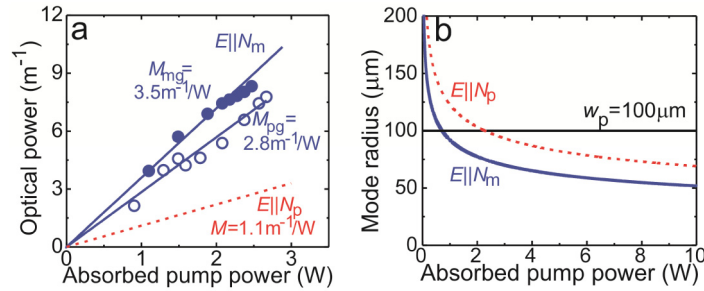


Fig. 3. (a) Optical power of the thermal lens in Yb:KLuW for light polarizations $E \parallel N_m$ (symbols: experimental data, solid lines: linear-fits) and $E \parallel N_p$ (dashed line, calculation); (b) calculated radius of the intracavity mode of the Yb:KLuW microchip laser.

An important feature of the thermal lens is a low difference of the M -factors along the N_p and N_m -axes, denoted as astigmatism degree S which is $0.7 \text{ m}^{-1}/\text{W}$ for Yb:KLuW, or 20% if expressed in the form S/M . In other words, the thermal lens is closer to a spherical one ($S/M = 0$) rather than to a purely cylindrical ($S/M = 100\%$). The astigmatism is directly linked to the beam ellipticity [22]. Therefore the observed near-spherical thermal lens plays a key role in achieving near-circular intensity profile of the Yb:KLuW microchip laser, in particular at high output powers.

The evolution of the emission spectra for several pump levels ranging from close to the laser threshold up to the highest P_{abs} of $\sim 10 \text{ W}$ are depicted in Fig. 4 for $T_{\text{OC}} = 5$ and 10%. Starting with one peak in the spectrum near the laser threshold, the spectrum gets broadened and multiple peaks are observed. The dominant wavelengths for the 5% and 10% OC are 1051.4 and 1048.6 nm, respectively.

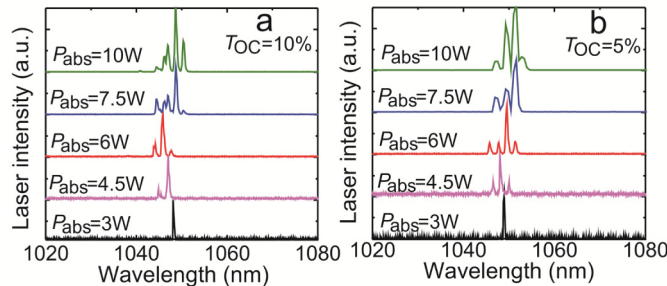


Fig. 4. Evolution of the emission spectra of the Yb: KLuW microchip laser for several pump levels; (a) $T_{\text{OC}} = 10\%$, (b) $T_{\text{OC}} = 5\%$.

In the following section we consider the laser characteristics when using $T_{\text{OC}} = 1\%$. The output power for this OC is lower than for 5 and 10% with a maximum of 3.6 W and a slope efficiency of 47% (Fig. 2). In contrast to the 5% and 10% OC, with $T_{\text{OC}} = 1\%$ the laser shows a different spectral and polarization behavior. The polarization state of the laser output is linear, $E \parallel N_m$, for $P_{\text{abs}} < 5.7 \text{ W}$, but an orthogonal component with $E \parallel N_p$ starts to oscillate for higher absorbed pump powers. With further increase of the pump level, a roll-over for m -polarized emission is observed, Fig. 5(a). At the maximum pump level, m and p -polarized emissions correspond to 74% and 26% of the total output. However, no deviation of the input-output dependence from the linear one is observed. The polarization-switching is apparent also in the laser emission spectrum, Fig. 5(b). The spectra of the m and p

polarization components are different, with the dominant wavelengths of 1063.6 nm (m) and 1059.6 nm (p), which is consistent with the emission properties of Yb:KLuW [4].

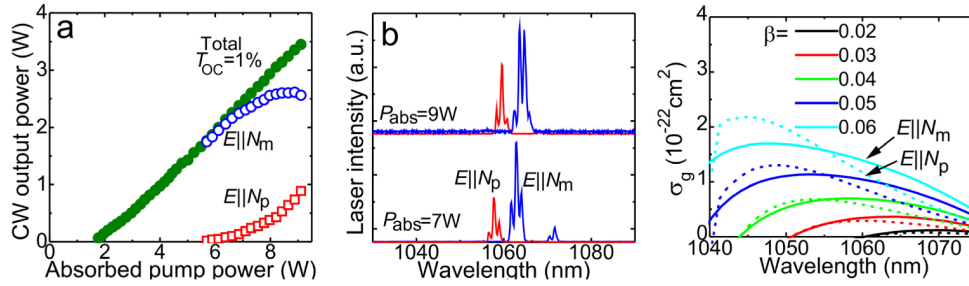


Fig. 5. Evidence of polarization-switching in the Yb:KLuW microchip laser at low inversion levels. (a) Output vs. absorbed pump power (filled symbols: total output, open symbols: contributions of $E \parallel N_m$ and $E \parallel N_p$); (b) laser spectra – simultaneous emission of both polarizations; (c) anisotropy of gain cross-sections, σ_g , for inversion ratios $\beta \leq 0.06$.

In order to explain the laser behavior when using $T_{OC} \leq 1\%$, we analyze the anisotropy of the gain cross-sections σ_g of Yb:KLuW for $E \parallel N_m$ and $E \parallel N_p$ at the corresponding low inversion ratios. In Fig. 5(c) σ_g is calculated for $\beta \leq 0.06$. The spectral dependence of σ_g for m and p -polarization is very similar. However, the local maximum in the gain spectrum of the m -polarization corresponds to longer wavelengths compared to the p -polarization. Additionally both maxima move spectrally to shorter wavelengths with increasing inversion level. Similar behavior could be in principle expected also for higher output coupling because the gain anisotropy persists also at higher inversion levels but was not experimentally observed with $T_{OC} = 5\%$ and 10% for the available pump powers, see Fig. 2.

Recently, polarization switching between N_m and N_p oscillating states was observed for N_g -cut Yb:KGdW [23]. A similar effect was detected in [24] and explained in [25] for an a -cut Yb:CALGO crystal. For Yb:KLuW, it was predicted theoretically in [26]. In all cases, polarization-switching was attributed to the anisotropic thermal lens introducing different losses for the two orthogonal polarizations. We calculated the optical power of the thermal lens for Yb:KLuW and $E \parallel N_p$, and it is shown as dashed line in Fig. 3(a) (see details in [26]). The thermal lens for $E \parallel N_p$ is always positive, i.e. it provides the desired mode stabilization, but weaker compared to the m -polarization, with an M -factor being only $1.1 \text{ m}^{-1}/\text{W}$. The latter leads to even better matching between pump and laser modes, Fig. 3(b). Hence, no change in the laser performance is detected when increasing the pump power. Such behavior was called “magic” mode stabilization in [24].

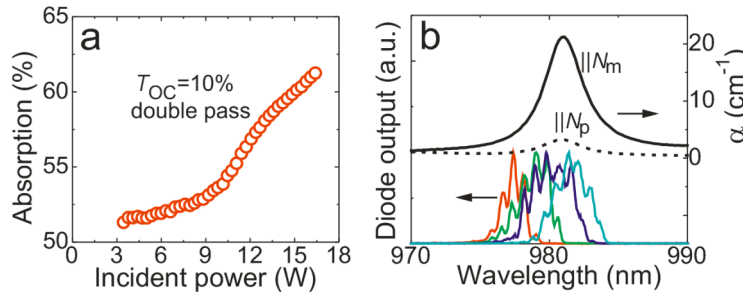


Fig. 6. (a) Overall pump absorption in the 3 at.%Yb:KLuW laser crystal in dependence on the incident pump power, $T_{OC} = 10\%$; (b) diode pump laser emission spectrum for $P_{inc} = 3$ (red), 9 (green), 12 (black) and 15 (blue) W and the main absorption peak of Yb^{3+} -ions in KLuW.

The absorption of the pump radiation in the studied microchip laser was dependent on the pump level, see Fig. 6 ($T_{OC} = 10\%$). This is related to the red-shift of the diode emission

spectrum for increased pump power, P_{inc} , which is shown in Fig. 6 (inset) together with the absorption spectra of 3 at.%Yb:KLuW for $E \parallel N_m$ and N_p . The red-shift of the diode emission leads to better spectral matching to the main absorption peak of Yb:KLuW centered at 981.0 nm. Thus, the overall (two-pass) absorption is increased from 51% ($P_{\text{inc}} = 3.5\text{W}$) to 62% ($P_{\text{inc}} = 16.5\text{W}$). This effect was considered when plotting the input-output dependences in Figs. 2 and 5(a). Maximum optical-to-optical efficiency of the Yb:KLuW microchip laser with respect to the incident diode power is then 27% (for $T_{\text{OC}} = 10\%$).

Another host often applied for Yb-doped microchip lasers is YAG, in the form of a single crystal or ceramics. For longitudinal pumping multi-watt TEM₀₀ output with > 60% slope efficiency was obtained in CW operation [27, 28] (edge-pumping produced > 100 W output with a multimode beam, $M^2 \sim 20$ [29]). Yb:LuAG and Yb:YAB microchips were also investigated with slightly performance [30, 31]. The present results are comparable to those achieved with Yb:YAG although KLuW exhibits roughly three times lower thermal conductivity.

In addition, the benefit of KLuW as compared with YAG is the high possible Yb doping level (up to 100 at.% (KYbW); absorption length: 13 μm at $\sim 980\text{ nm}$ for $E \parallel N_m$ [7]) which is not accompanied with a drop of the thermal conductivity. This would be one way for a more compact microchip laser design. Ultimately, the efficiency for such extreme aspect ratios will be limited, similar to the situation found in thin-disk lasers, by amplified spontaneous emission (ASE) and special measures will be needed to suppress parasitic oscillations [32].

An increase of the slope efficiency of the Yb:KLuW microchip laser can be achieved with a proper matching of pump and laser mode (estimated "optimal" w_p is $50 \pm 5\ \mu\text{m}$ in our design). We believe that this can improve the slope up to > 80%, limited only by the laser quantum defect ($\eta_h \sim 0.07$, in our case). Further power scaling is possible by optimization of pump absorption with variation of the Yb content and crystal length (to utilize the benefits of side-cooling), as well as the use of synthetic diamond as a heat spreader.

4. Conclusions

We demonstrated multi-watt microchip laser operation of an Yb-doped double tungstate crystal, using KLuW as host. With a 2.6 mm-thick 3 at.%Yb:KLuW crystal cut along the N_g -axis of the optical indicatrix, maximum CW output power of 4.4 W was extracted at the wavelength of 1049 nm with a slope efficiency of 65% (with respect to the absorbed pump power). The thermal mechanism of mode stabilization in the microchip cavity was verified. The microchip laser generated linearly polarized emission in near-circular TEM₀₀ mode with $M^2 < 1.1$. No degradation of the beam quality up to 16 W of incident pump power was observed. Due to the low intracavity losses, multi-watt operation at laser wavelengths beyond 1063 nm was also achieved. Polarization-switching between N_m and N_p oscillating states was observed for low inversion levels ($T_{\text{OC}} \leq 1\%$).

Acknowledgments

This work was supported by the Spanish Government under project MAT2011-29255-C02-02, MAT2013-47395-C4-4-R and by Generalitat de Catalunya under project 2014SGR1358.